Title: Oxidative Dehydrogenation of Ethane: A Chemical Looping Approach

Authors: Luke Micheal Neal, Ph.D.; Seif Yusuf; John A Sofranko; Fanxing Li

To be cited as: 10.1002/ente.201600074

Link to VoR: http://dx.doi.org/10.1002/ente.201600074

Oxidative Dehydrogenation of Ethane: A Chemical Looping Approach

Luke M. Neal,[a] Seif Yusuf,[# a] John A. Sofranko,[b] and Fanxing Li*[a]

Abstract: The current study investigates a chemical looping based oxidative dehydrogenation (CL-ODH) concept for ethane to ethylene conversion. In this cyclic redox scheme, an oxide-based redox catalyst is used to selectively combust hydrogen from ethane dehydrogenation. Since the hydrogen product limits ethane conversion, *in-situ* oxidation of hydrogen enhances ethane conversion and ethylene yield. Moreover, heat required in ODH is compensated by re-oxidation of the oxygen-deprived redox catalyst, enabling auto-thermal operation for the overall process. Compared to steam cracking, CL-ODH can potentially achieve higher efficiency with lower CO_2 and NO_x emissions. Silica and magnesia supported manganese oxides are investigated. It is determined that unpromoted Mn/SiO_2 and Mn/MgO redox catalysts exhibit low selectivity towards ethylene. Addition of promoters such as Na and W renders effective redox catalysts with satisfactory activity, selectivity, oxygen carrying capacity, and redox stability.

Introduction

The combustion of fossil fuels is the primary source of anthropogenic CO_2 and NO_x emissions. Although significant amounts of CO_2 are emitted from combustion of liquid transportation fuels, CO_2 control for such mobile sources is technologically challenging. In comparison, stationary sources such as combustion based power plants and industrial production account for over 50% of fossil fuel related carbon emissions in the United States.[1] Therefore, development of effective carbon capture and emission reduction techniques for stationary emission sources represents one of, if not the, most important approach to address the ever increasing concerns over global climate change and NO_x related smog issues. Although proven CO_2 control technologies such as chemical and physical solvent based absorption processes can be applicable for CO_2 capture in fossil fuel combustion power plants, such processes are highly capital and energy intensive.[2] 90% CO_2 capture from a coal-fired power plant can reduce the electricity production by 42% while increasing the cost of electivity by up to 90%.[2,3] Among the various carbon capture technologies investigated to date, chemical looping combustion (CLC) represents one of the more promising approach.[4–13] A simplified schematic of the CLC process is shown in Figure 1. Briefly, a carbonaceous fuel is converted to CO_2 and water in a fuel reactor with lattice oxygen from a metal oxide based oxygen carrier. The oxygen carrier is subsequently transferred to an air reactor where it is re-oxidized and the heat for power generation is produced. The high concentration CO_2 flue gas stream from CLC allows for efficient CO_2 separation.[3,11] In addition, the air reactor in CLC is operated at relatively low-temperature via flameless "combustion" of reduced oxygen carriers, leading to significantly reduced NO_x production,[14] thereby eliminating the needs for selective catalytic reduction (SCR). These distinct advantages offered by CLC have spurred extensive research and development activities over the past two decades both in terms of oxygen carrier development [15–20] and process scale up and demonstrations.[21–26]

Figure 1. Schematic of the CLC process

Despite the significant recent advances in CLC, a number of obstacles hinder its near-term implementation at commercial scales: (i) Economies of scale dictate that typical power plants need to process fossil fuels at a significant capacity. This translates into high solids circulation rates for typical CLC oxygen carriers, ranging between 3,600 – 30,000 tons/hour with inventories of 400-2,500 tons;[11] (ii) While CLC addresses the capture aspect of the carbon capture, utilization, and storage (CCUS) process, suitable methods of utilizing or safely storing large quantities of captured carbon is yet to be fully demonstrated;[10,27–29] (iii) Lack of concerted efforts to enforce CO_2 regulations at a global scale also limits the development of CO_2 capture technologies. Therefore, continued research and development efforts are desired for widespread implementation of CLC.

In addition to fossil fuel combustion and CO_2 capture, the concept of chemical looping has been applied to produce value-added chemical products instead of CO_2. One such example is the chemical looping reforming (CLR) process[6,30–34]. The oxygen carrier in CLR partially oxidizes methane into CO and H_2 in the fuel reactor. The reduced oxygen carrier is subsequently regenerated with air, producing heat that compensates the heat requirements for methane partial oxidation. The oxygen carrier, a.k.a. redox catalyst, in CLR also functions as a catalyst. Compared to conventional steam and partial oxidation (PO_x) reforming processes, CLR has the potential to be more efficient since the energy requirements for steam generation, endothermic steam reforming, or air separation are eliminated.[6] While CLR has the potential to be more efficient and economical than traditional reforming, it faces challenges such as syngas selectivity, redox catalyst cost, and coke formation. Pröll et al. demonstrated CLR in a 140 kW_{th} pilot plant using NiO based redox catalysts and reported syngas selectivities lower than 70%.[35] Significant research efforts have been devoted to finding redox catalyst, or integrated co-generation processes to overcome these limitations. [6,31,32,36,37] We reported highly engineered materials that can achieve syngas yield over 90% with good coke resistance and high oxygen capacities.[32,37–39] However, testing of these high performance catalysts in pilot scale reactors have yet to be performed. Moreover, the economic advantage of CLR compared to state-of-the-art methane reforming processes can be limited considering the

[a] Dr., LM, Neal, S, Yusuf[#], Prof., F, Li[*]
Department of Chemical & Biological Engineering
N.C. State University
911 Partners Way, Raleigh, NC 27695-7905
[#] Co-first Author
[*] fli5@ncsu.edu

[b] Dr., JA, Sofranko
EcoCatalytic Technologies
LLC 9 Deer Park Drive, Suite J-1. Monmouth Junction, NJ 08852

value of syngas relative to methane. Alternative approaches that can convert low value, saturated hydrocarbons, such as ethane, to higher value products such as olefins with improved efficiency and reduced carbon footprint are therefore highly desirable.

The current study investigates a chemical-looping based approach for oxidative dehydrogenation of ethane (ODH) (Figure 2). In the following sections, the proposed CL-ODH process is explained in detail. This is followed by proof-of-concept testing of potential redox catalysts for CL-ODH. The results indicate that promoted manganese oxide on SiO_2 and MgO supports can be effective redox catalysts. Among the redox catalysts investigated in the current study, sodium tungstate promoted Mn/MgO renders particularly high ethylene yields with high selectivity and satisfactory oxygen storage capacity and redox stability over multiple redox cycles.

CL-ODH Process Overview:

Commodity chemicals such as ethylene are often overlooked for their contributions to CO_2 and NO_x emissions. Current world demand for ethylene amounts to more than 140 million tons/year.[40] Commercial ethane to ethylene processes are carried out through steam cracking (Eq. 1). The highly endothermic cracking reaction (143 kJ/mol), high reaction temperatures (up to 1,100 ˚C), and significant downstream separation loads make commercial steam cracking very energy/carbon intensive.[41] Production of 1 ton of ethylene requires 16 GJ of thermal energy and results in approximately 1.2 tons of CO_2 emissions.[42] A widely studied alternative for steam cracking is ethane oxidative dehydrogenation (ODH) in which ethane and gaseous oxygen are co-fed in the presence of a heterogeneous catalyst (Eq. 2).[43–46] The use of gaseous oxygen to oxidize hydrogen byproducts renders an exothermic dehydrogenation process with higher single-pass ethane conversion. Ren et al. estimated that conventional ODH consumes ~35% less thermal energy when compared to conventional steam cracking processes.[42] However, the need for air separation, which is capital intensive and consumes ~1/3 of the process energy,[42] limits the comparative advantage of ODH relative to steam cracking. In addition to the requirement of ASU, safety concerns over co-feeding oxygen and ethane as well as the limits in product selectivity hinder industrial application of ODH processes.

We propose a CL-ODH process that addresses the limitations of conventional steam cracking and ODH processes (Fig. 2). Similar to CLR, the CL-ODH process is carried out via two steps. In the first step, the oxygen for ODH is supplied by the lattice oxygen of a redox catalyst (Eq. 3) in the ODH reactor. The ODH reaction in the presence of metal oxide can be endothermic (Eq. 3). The heat required by CL-ODH is supplied by the second step, in which the reduced redox catalyst is regenerated via an exothermic oxidation reaction (Eq. 4). Such a reaction heats up the redox catalyst particles, which convey the heat to the ODH reactor through recirculation.

Steam Cracking (main reaction)

Eq. (1) $C_2H_6 \leftrightarrow C_2H_4 + H_2$ $\Delta H^{850\,^{\circ}C}$ =143 kJ/mol[a]

Oxidative Dehydrogenation (ODH)

Eq. (2) $C_2H_6 + \frac{1}{2}O_2 \rightarrow C_2H_4 + H_2O$ $\Delta H^{850\,^{\circ}C}$ =-105 kJ/mol[a]

Chemical Looping-ODH (CL-ODH, MnO and Mn_3O_4 are Shown as an Example)

Eq. (3) $C_2H_6 + Mn_3O_4 \rightarrow C_2H_4 + H_2O + 3 \bullet MnO$ $\Delta H^{850\,^{\circ}C}$ =118 kJ/mol[a]

Eq. (4) $3 \bullet MnO + \frac{1}{2}O_2 \rightarrow Mn_3O_4$ $\Delta H^{850\,^{\circ}C}$ =-223 kJ/mol[a]

[a] Calculated in HSC Chemistry 6.0

Olefin production via a chemical-looping concept was explored by ARCO Chemical for oxidative coupling of methane (OCM) [47–51]. It was reported that a redox mode of operation leads to higher C_{2+} selectivity when compared to an oxygen co-feed mode using Mn based oxide catalysts. The per-pass C_{2+} yield, however, is generally limited to ~20%.[52] The low product yield and high energy consumption for methane and C_2 separation affect the economic attractiveness of such a process. Adaptation of vanadium oxide based based oxygen carriers to chemical looping ODH at low-temperatures (~500-600 °C) has also received attention.[53–57] These systems are generally limited to low conversions to maintain selectivity, and the requirement for supports to maintain activity limits the oxygen capacity of vanadium based oxygen carriers. Effective redox catalysts with high oxygen capacity and selectivity are therefore highly desired for CL-ODH.

Figure 2. Chemical Looping-Oxidative Dehydrogenation of ethane (CL-ODH). The ODH reactor serves as the fuel reactor.

Figure 2 illustrates a process schematic of CL-ODH. In such a scheme, ethane is fed along with a redox catalyst into an ODH reactor, where lattice oxygen is used to partially oxidize ethane to water and ethylene. The reduced redox catalyst is subsequently regenerated with air in the air reactor (Eq. 4). The exothermic reaction heats the catalyst particles, which convey sensible heat into the ODH reactor. The product gas stream from the ODH unit is rapidly cooled and then compressed. This is followed with drying, acid gas removal, cooling, and fractionation to recover ethylene and other value-added products. Unreacted ethane is recycled into the ODH feed stream.

Comparison of CL-ODH with Steam Cracking and ODH

The CL-ODH approach (Figure 2) offers several advantages over the conventional steam cracking process. For instance, H_2 product limits the equilibrium conversion of ethane in steam cracking. Selective oxidation of H_2 to H_2O, enabled by the CL-ODH redox catalyst, can lead to significantly improved single pass yield of ethylene. Increase in single-pass yield, along with H_2 combustion, result in significantly lowered molar flow rate of non-condensable gaseous products from ethane conversion. Therefore, energy consumption for downstream compression and separation processes are decreased for CL-ODH. Moreover, steam cracking is highly endothermic. Combustion of fuel gases such as methane and hydrogen byproduct in conventional cracking leads to significant CO_2 and NO_x emissions.[58] In comparison, CL-ODH allows auto-thermal operations through indirect combustion of hydrogen byproduct. As a result, the overall efficiency loss is reduced. Moreover, indirect flameless combustion of hydrogen in CL-ODH significantly reduces CO_2 and NO_x emissions.[59] Additionally, steam cracking requires significant steam dilution of the ethane feed to suppress coke formation. Even so, crackers need to be periodically shut down for coke burn-off. In comparison, CL-ODH eliminates the needs

for steam dilution and allows continuous process operations. Compared to oxygen co-fed ODH, CL-ODH eliminates the capital and energy intensive air separation units (ASU). It also eliminates the direct contact between gaseous oxygen and ethane. As a result, the selectivity and operability of the ODH process can be improved.

Results and Discussion

Support Selection Rationale

In this work we focus on two manganese based redox catalyst systems, i.e. MnO_x/SiO_2 and MnO_x/MgO. The Effects of adding sodium and sodium tungstate promoters are also investigated. Manganese oxide is selected as the redox catalyst due to its known oxygen storage capacity,[60] and supported MnO_x have been shown to be an active heterogeneous catalysts for ODH reactions.[61–65] Silica and magnesia are selected as the supports since they are frequently used for OCM and ODH reactions under an oxygen co-feed mode.[61–65] Sodium and sodium tungstate have also been shown, in previous studies, to be effective promoters for manganese-silica and manganese-magnesia based heterogeneous catalysts for OCM reactions. [61–65]

CL-ODH Catalyst Selection Criteria

To realize the potential efficiency gains and emissions reductions, redox catalyst selection for CL-ODH is of critical importance. The redox catalyst needs to not only have satisfactory redox activity/stability and oxygen storage capacity but also be largely inactive for non-selective oxidation of hydrocarbon feedstock and products. Such a requirement is in distinct contrast with CLC oxygen carriers which seek to oxidize hydrocarbon fuels into CO_2. In addition to the ability to inhibit non-selective hydrocarbon oxidation, the redox catalyst should have high activity and selectivity for H_2 combustion. Hydrogen combustion by the redox catalyst is critical for the proposed CL-ODH concept since it contributes directly to the reduction of the redox catalyst during the ODH step (Eq 3). Since the overall heat of reaction for the process is satisfied by the re-oxidation of the redox catalyst reduced in the ODH step (Eq. 4), hydrogen conversion and selectivity directly relates to the heat balance of the overall process (Eq. 2). Moreover, H_2 removal can lead to higher single pass conversion of ethane provided that the rate of H_2 removal reaction is comparable to that of thermal cracking. Therefore, redox oxides that can selectively and actively combust H_2 in the presence of ethane and ethylene would be suitable for the proposed CL-ODH process. Overall energy balance and equilibrium calculations indicate that H_2 conversion of 60% or higher is desirable for the CL-ODH process. From a reaction kinetics standpoint, such a H_2 conversion should be achieved in the order of 0.5 s at 850 °C , which is the typical residence for industrial stream cracking.[58]

Figure 3. XRD patterns of **a)**. The Mn/SiO_2 system catalysts and **b)**.the Mn/MgO system catalysts.
[a] PDF# 00-024-0734, [b] PDF# 00-041-1442, [c] PDF# 00-003-0271, [d] PDF# 04-008-8508, [e] PDF# 01-074-1903, [f] PDF# 04-005-5745

The XRD pattern of the unpromoted Mn/SiO_2 catalyst is consistent with manganese oxides on poorly crystalline silica (Figure 3). However, the inclusion of the Na-containing promoters induces the SiO_2 support to change to a cristobalite phase with a sharp drop in surface area (135 vs 1.34 m^2/g, Table 1). Both Mn/MgO samples indicate the formation of Mg_6MnO_8. Although the MgO's XRD pattern would be obfuscated by that of Mg_6MnO_8, the lack of crystalline Mn oxide to account for the Mn loading indicates that most, if not all, Mn is integrated into the Mg_6MnO_8 structure. This catalyst system is, thus, more properly described as a Mn/Mg mixed oxide. Despite this mixed oxide formation, the Mn/Mg catalyst have higher surface areas than the sodium and sodium tungstate promoted Mn/SiO_2 samples. BET indicates that the as prepared Mg_6MnO_8 catalyst and sodium tungstate doped Mg_6MnO_8 have surface areas of 4.3 and 3.5 m^2/g respectively. Although the surface areas of the Mg_6MnO_8 systems are low when compared to supported metal catalysts, many oxide catalysts have comparable surface areas. Such surface areas are also typical for oxygen carriers in chemical looping processes [20,66,67] where oxide activity tends to correlate more with internal oxygen transport properties than surface area.[20,32,39]

Table 1. *BET surface areas of redox catalysts investigated in the current study*

Dopant	SiO_2 Support	MgO Support
None	135 m^2/g	4.34 m^2/g
Na	1.15 m^2/g	n/a
Na Tungstate	1.36 m^2/g	3.56 m^2/g

Figure 4. TGA of redox cycles 1 through 5 for **a).** $Na/Mn/SiO_2$ and **b).** Mn/MgO reduced in 10% H_2 and oxidized in 10% O_2.

Catalyst Characterization and Redox Performance

To probe the oxygen storage capacity of the two redox catalyst systems without complicating side reactions, redox cycles with 10% hydrogen for oxide reduction and 10% oxygen for regeneration are performed isothermally at 850 °C. Figure 4 illustrates the redox behavior of the unpromoted Mn/MgO and sodium promoted Mn/SiO_2 samples. A sodium promoted Mn/SiO_2 sample was chosen due to the formation of a cristobalite phase after Na addition, which leads to a significant drop in surface area (Figure 3, Table 1). Both samples showed stable performance over multiple cycles. As shown in Figure 5, the SiO_2 and MgO supported sample have oxygen capacity of 1.0 wt. % and 4.1 wt. % respectively at 850 °C. Such oxygen storage capacities are deemed acceptable for chemical looping reactions.[6] Both samples also exhibit satisfactory oxygen recyclability over the 5 redox cycles performed, indicating promising redox properties for the proposed CL-ODH reactions. In terms of reduction rates at 850 °C, the SiO_2 supported sample exhibits significantly lower activity for the oxidation reaction when compared with the Mn/MgO sample, with significant weight gain still occurring after 30 min in 10% O_2.

Figure 5. TGA weight loss/reduction rates in 10% hydrogen at 850 °C for a). $Na/Mn/SiO_2$ and b). Mn/MgO

Compared to oxidation, the reduction rate of the redox catalyst is more important as it affects the efficiency of hydrogen removal for the ODH step. The necessary reduction rate of the redox catalyst will vary depending upon product distributions and the particle density of the bed. Simple order of magnitude calculations indicate that a minimum reduction rate greater than 0.4 wt.% oxygen / minute over a reasonable range of oxygen utilization is desirable based upon cracking rates at 850 °C. As

Table 2. *Conversion/selectivity for redox catalyst 4500 h^{-1} 850 C 5 ml injection of 15% Mn catalyst*

Catalyst	*Ethane Conversion*	*Ethylene Selectivity*	*CO Sel.*	*CO_2 Sel.*	$\frac{mol\ H_2}{mol\ C_2H_4}$ [a]	*Water Sel.*	$\frac{r_{O,H_2O}}{r_{O,CO_x}}$
Blank	46%	93%	0%	0%	101%	0%	NA
Mn/SiO_2	51%	88%	1.2%	1.1%	61%	43%	6.9
$Na/Mn/SiO_2$	47%	92%	0.53%	0%	51%	51%	47
$Na\text{-}W/Mn/SiO_2$	45%	90%	0.65%	1.2%	12%	88%	13
Mn/MgO	85%	18%	0%	77%	18%	99%	9.8
Na-W/Mn/MgO	64%	86%	0.86%	1.4%	22%	81%	16

[a] *Due to net hydrogen production from the formation of C_{3+} hydrocarbon and CO_x byproducts, this adds to >100% with water selectivity.*

can be seen in Figure 5, both the MgO and SiO_2 samples exceeded the 0.4 wt.% oxygen/min lower bound for usability in CL-ODH, with the Mn/MgO sample being more than an order of magnitude higher than the threshold.

The SiO_2 supported sample underperformed the MgO supported sample in terms of reduction rate and oxygen capacity. While potentially viable, the reduction rate of promoted Mn/SiO_2 for CL-OCM could limit the range of operating conditions, diminishing the degree of freedom for looping reactor design and operations. The exceptional reduction rate of the Mn/MgO makes it more interesting for CL-ODH than the SiO_2 supported catalysts. Its better performance cannot be attributed solely to higher surface area. BET (Table 1) shows that, while exceeding that of the promoted SiO_2 catalyst, its surface area still requires oxygen to be supplied rapidly from the bulk. The Mg_6MnO_8 structure formed, thus, appears to have excellent solid-state oxygen transport properties. The promoted Mn/MgO system, thus, is a very promising redox catalyst for CL-ODH.

Catalyst ODH Performance

Table 2 and Figure 6 summarize ODH performance of the redox catalysts along with background ethane cracking reactions in a blank experiment with alumina grits. All of the redox catalysts show significant activity towards water formation, with ethane conversions similar to or larger than thermal cracking in a blank tube. For most catalysts, the overall hydrocarbon product distribution is consistent with thermal cracking in the blank (Table 3). Methane, acetylene, and 1,3-butadiene represent the majority of the hydrocarbon byproducts. The stoichiometries of these byproducts are included in hydrogen/water balance calculations. Trace amounts of CO_x are observed by a mass spectrometer during re-oxidation, and tar formation (from heavy hydrocarbon products) is observed at the outlet of the reactor. However, integration of signals, and internal standard experiments indicate that the yield of these products are not significant.

An important requirement for CL-ODH catalyst is its ability to selectively combust H_2 as opposed to hydrocarbons, since formation of low value CO_x products are not desired. Mass spectroscopy shows that the selectivity improves as oxygen is pulled out of the sample, but the concentration of hydrogen in the effluent also increases. The selectivity and activity trends between samples generally hold over pulse times long enough to significantly deplete usable oxygen. Silica supported manganese oxide samples show good selectivity towards hydrogen oxidation vs. CO_x formation. For the unpromoted and sodium promoted samples, the ratios of active lattice oxygen for water formation relative to CO_x formation are 6.9:1 and 47:1 respectively but have water selectivities of less than 60%. In the case of the sodium tungstate promoted silica sample, such a ratio is 13:1. Moreover, hydrogen conversion exceeds 60%, making it suitable for the CL-ODH application from an energy balance viewpoint based on earlier discussions. However, for this sample, the ethane conversion is not significantly higher than the thermal background (Blank Table 1), suggesting little catalytic or equilibrium shift enhancement of the conversion. This is consistent with the relatively slow H_2 combustion kinetics for the silica supported samples.

Figure 6. Conversion, selectivity and yield for ODH of redox catalyst

Table 3. *Representative GC results of thermal cracking (Blank) and ODH*

	Blank	$Na\text{-}W/Mn/SiO_2$
Name	Vol %	Vol%
H_2	30.1%	4.7%
Methane	2.1%	3.5%
CO	0.0%	0.5%
CO_2	0.0%	1.0%
Acetylene	0.1%	0.1%
Ethane	37.5%	51.4%
Ethylene	29.7%	37.9%
Propylene	0.2%	0.3%
N-Butane	0.1%	0.1%
1,3-Butadiene	0.2%	0.4%

Table 4. *Mass spectroscopy characterization of CL-ODH over sodium tungstate promoted Na-W/Mn/MgO at 850° C and 4500 h-1 for 25 cycles*

Cycle #	*Ethane Conversion*	*Ethylene Selectivity[a]*	*Ethylene Yield*
2	66%	93%	61%
5	66%	90%	60%
11	65%	93%	61%
25	66%	93%	61%

[a] Mass spectroscopy gives higher apparent ethylene selectivity due to neglect of C_{3+} products and very poor resolution of CO caused by convolution of characteristic peaks with ethane, ethylene, and CO_2 that occurs with electrical ionization

The MgO supported systems are significantly more active in terms of ethane conversion and H_2O/CO_x production. Without dopant, 15% Mn/MgO is a highly effective ethane combustion catalyst, burning 67% of carbon in the ODH reaction step with high selectivity to CO_2. As such it is unsuitable for ODH. The Na-W/MnMgO catalyst was significantly more selective towards hydrogen oxidation over CO_x formation (16:1 on an oxygen basis) while maintaining conversions significantly higher than the thermal background (64% vs 46%). Although the selectivity to

water over hydrogen is somewhat less than the sodium tungstate promoted Mn/SiO_2 catalyst (81% vs 88%), its higher efficiency in ethane conversion makes it more promising.

To test the sodium tungstate doped Mn/MgO catalyst for long term stability a 25 cycle test monitored with mass spectroscopy is performed (Table 4). The Na-W/Mn/MgO redox catalyst's performance over these cycles is very stable. No significant deactivation or selectivity loss is observed and ethylene yield remains consistent.

Conclusions

The current study discusses a chemical looping–oxidative dehydrogenation (Cl-ODH) concept for ethylene generation. CL-ODH has several potential advantages over conventional ethane dehydrogenation technologies since it significantly reduces the energy requirements for ethane conversion and increases single pass ethylene yield. Indirect, flameless combustion of H_2 byproduct also leads to significantly lower CO_2 and NO_x emissions. Two redox catalyst systems, i.e. SiO_2 and MgO supported Mn oxides are investigated for the aforementioned application. Effects of adding sodium and sodium tungstate promoters are also studied. Two redox catalysts are found to be potentially suitable for the proposed CL-ODH process. These redox catalysts, i.e. sodium promoted Mn/SiO_2 and sodium tungstate promoted Mn/MgO, show adequate oxygen storage capacities of up to 4.1 wt.%. In addition, both redox catalysts are capable of selectively combusting hydrogen. Sodium tungstate promoted Mn/MgO is especially promising, showing fast oxygen donation, high selectivity, and good redox stability. Single pass yield of ethylene is increased by 12% in the presence of the redox catalyst. In addition, H_2O selectivity is found to be over 80%. Overall, sodium tungstate promoted Mn/MgO is a promising redox catalyst candidate for the CL-ODH process to meet the growing world demand for clean ethylene.

Experimental Section

Catalyst Synthesis

All catalysts are synthesized through an incipient wetness impregnation method. For the unpromoted catalyst, manganese (II) nitrate (Sigma-Aldrich) is dissolved in DI water and then mixed with the support material, silica pellets (Alfa Aesar), or magnesium oxide powder (Materion) in order to create 15% wt. manganese on the metal oxide support. The resulting mixture is stirred to obtain a uniform distribution and then dried overnight at 80°C. Next, the catalyst is calcined in air: first the temperature is ramped to 450°C at a rate of 5°C/min and then held for 3 hours. The temperature is then ramped to 900°C at a rate of 5°C/min and held for 8 hours. The catalyst is then allowed to cool down to room temperature. After cooling, a mortar and pestle is used to grind the catalyst and sieves are used to separate the different particle sizes.

The two dopants chosen for this study are sodium and sodium tungstate and their respective precursors for these dopants were sodium nitrate (Fisher) and sodium tungstate dihydrate (Sigma-Aldrich). For each of these catalysts, the final doping level of sodium is 1.7 wt. %. For the sodium promoted catalyst, the sodium and manganese precursors are dissolved together in DI water and then mixed with the support material as in the unpromoted catalyst preparation. For the sodium tungstate promoted catalyst, the impregnation is done in two steps to prevent precipitation of the tungsten precursor. First manganese (II) nitrate was mixed with the support material as with the unpromoted catalyst. After drying at 80°C overnight, the catalyst is quickly heated to 200°C in order to decompose the nitrate. Afterwards, sodium tungstate dihydrate is dissolved in DI water and then mixed with the catalyst and dried overnight at 80°C. Following calcination the samples are sieved.

Catalyst Phase Identification/BET

Phase identification of the freshly synthesized catalysts is performed using Powder X-Ray Diffraction (XRD, Rigaku SmartLab X-ray Diffractometer with Cu Kα λ = 0.1542 nm radiation operating at 40 kV and 44 mA). A scanning range of 10-80° (2Θ) with a step size of 0.1° holding for 3.5s at each step is used to generate XRD patterns.

Adsorption isotherms are collected on a Micromeritics ASAP 2010 at 77 K using N_2 as the adsorbent gas. The surface areas are evaluated using Brunauer–Emmett–Teller (BET) theory. All of the samples are degassed at 473 K under vacuum before the measurements.

Ethane ODH Testing

ODH of ethane is performed in a U-tube reactor in order to reduce reactor dead volume and to minimize back mixing. The quartz U-tube has a ¼'' O.D and ⅛" I.D. and is loaded with 0.5 g. of catalyst particles that are in the range of 425μm and 850μm. 16 mesh white alumina grit is loaded on each side of the catalyst particles to prevent blowout of the catalyst, and limit the gas volume of the heated zone reactor zone. For the blank runs the entire tube is packed with the white alumina grit to maintain consistent gas residence times. The quartz U-tube is heated by a tube furnace, and mass flow controllers with automated valve manifold are used to control the atmosphere in the reactor.

In order to determine the catalysts activity for the ODH of ethane, redox cycle experiments are performed. During the reduction step, the reactor environment is comprised of 80% ethane balance helium (5.0 grade). During the oxidation step the catalyst is regenerated in 10% oxygen balance helium. Before and after each reduction and oxidation step, 100% helium is flowed into the reactor to purge any remaining gasses. The reactor gas manifold is configured such that the total flow rate into the reactor does not change between purge and reduction steps. Before ODH testing, the catalysts are pretreated with 2 redox cycles comprising of a 3 minute reduction step and a 3 minute oxidation step at 900°C to obtain a redox catalyst with stabilized chemical and physical properties. The catalysts are then tested at 850°C and 75 sccm/min total flow rate during purge and reduction steps. A 5 second reduction time is used, which corresponds to an injection of 5 sccm ethane during each reduction. The oxidation step is 3 minutes and the purge steps are 5 minutes. The 75 sccm total flow rate during reduction and purge corresponds to a gas hourly space velocity of 4500 h^{-1}.

The products from the ODH reaction are collected in a gas sampling bag and characterized using a gas chromatograph (GC). An Agilent 7890 Series Fast RGA GC is used for product identification and quantification. It consists of a He/TCD channel for CO/CO_2 analysis, Ar/TCD channel for H_2 analysis, and an FID channel for hydrocarbon analysis. The system is calibrated

using a refinery gas calibration standard. The products ratios are calculated by integrating the signals for the characteristic peaks for each of these species. As internal standard experiments indicate that no significant coking or tar formation occurs under the conditions tested, mass balance is used to calculate the yields. Selectivities and conversions for carbonaceous species are calculated relative to the carbon mass balance. The total amount of hydrogen and water formed is calculated by hydrogen mass balance of all recovered species. The water selectivity is calculated relative to the amount of hydrogen recovered and the amount of total water and hydrogen expected by mass balance. The sodium tungstate promoted Mn/MgO catalyst is run for 25 continuous cycles, using a quadrupole mass spec (MKS Cirrus II) to monitor the gas elution in real time. The methane ethylene, ethane, and CO_2 signals are deconvoluted and integrated to calculate conversion and selectivity.

Thermogravimetric Analysis

In order to determine the behavior of the catalysts over multiple redox cycles, the unpromoted magnesium oxide supported catalysts and the sodium promoted silica supported catalyst are cycled on a TA Instruments SDT Q600 TGA. The sodium promoted silica supported catalyst is chosen over the unpromoted catalyst because the α-cristobalite is not observed in the unpromoted catalyst. Fresh catalysts are loaded into the instrument and then heated to 850°C at a rate of 20°C/min in a 10% O_2/90%Ar oxygen environment to maintain an oxidized catalyst. Next, the flow is switched to an inert environment for 15 minutes to remove oxygen and then a 10%H_2/90%Ar flow is introduced for 15 minutes to reduce the catalyst. After another 15 minute purge, 10%O_2/90%Ar is flowed again to re-oxidize the catalyst. 5 cycles are performed.

Acknowledgements

We acknowledge the funding support from Advanced Research Project Agency-Energy (ARPA-E) of the US Department of Energy (Grant DE-AR0000327) and the Kenan Institute.

Keywords: chemical looping •alkene • oxidative dehydrogenation • catalysis• dehydrogenation

[1] C. C. D. US EPA, "U.S. Greenhouse Gas Inventory Report," can be found under http://www3.epa.gov/climatechange/ghgemissions/usinventoryreport.html, accessed [15 Jan 2016]
[2] M. Zhao, A. I. Minett, A. T. Harris, *Energy Environ. Sci.* **2013**, *6*, 25–40.
[3] F. Li, L.-S. Fan, *Energy Environ. Sci.* **2008**, *1*, 248–267.
[4] J. Adánez, L. F. de Diego, F. García-Labiano, P. Gayán, A. Abad, J. M. Palacios, *Energy Fuels* **2004**, *18*, 371–377.
[5] J. Adánez, A. Cuadrat, A. Abad, P. Gayán, L. F. de Diego, F. García-Labiano, *Energy Fuels* **2010**, *24*, 1402–1413.
[6] J. Adanez, A. Abad, F. Garcia-Labiano, P. Gayan, L. F. de Diego, *Prog. Energy Combust. Sci.* **2012**, *38*, 215–282.
[7] H. Leion, T. Mattisson, A. Lyngfelt, *Energy Fuels* **2009**, *23*, 2307–2315.
[8] H. Leion, T. Mattisson, A. Lyngfelt, *Int. J. Greenhouse Gas Control* **2008**, *2*, 180–193.
[9] H. R. Kim, D. Wang, L. Zeng, S. Bayham, A. Tong, E. Chung, M. V. Kathe, S. Luo, O. McGiveron, A. Wang, et al., *Fuel* **2013**, *108*, 370–384.
[10] J. D. Figueroa, T. Fout, S. Plasynski, H. McIlvried, R. D. Srivastava, *Int. J. Greenhouse Gas Control* **2008**, *2*, 9–20.
[11] L.-S. Fan, in *Chemical Looping Systems for Fossil Energy Conversions*, John Wiley & Sons, Inc., **2010**, pp. i–xiv.
[12] Q. Imtiaz, D. Hosseini, C. R. Müller, *Energy Technol.* **2013**, *1*, 633–647.
[13] L.-S. Fan, F. Li, *Ind. Eng. Chem. Res.* **2010**, *49*, 10200–10211.
[14] M. Ishida, H. Jin, *Ind. Eng. Chem. Res.* **1996**, *35*, 2469–2472.
[15] M. Arjmand, H. Leion, T. Mattisson, A. Lyngfelt, *Appl. Energy* **2014**, *113*, 1883–1894.
[16] M. Arjmand, H. Leion, A. Lyngfelt, T. Mattisson, *Int. J. Greenhouse Gas Control* **2012**, *8*, 56–60.
[17] H. Gu, L. Shen, J. Xiao, S. Zhang, T. Song, D. Chen, *Combust. Flame* **2012**, *159*, 2480–2490.
[18] T. Song, J. Wu, H. Zhang, L. Shen, *Int. J. Greenhouse Gas Control* **2012**, *11*, 326–336.
[19] N. L. Galinsky, Y. Huang, A. Shafiefarhood, F. Li, *ACS Sustainable Chem. Eng.* **2013**, *1*, 364–373.
[20] N. L. Galinsky, A. Shafiefarhood, Y. Chen, L. Neal, F. Li, *Appl. Catal., B* **2015**, *164*, 371–379.
[21] F. Liu, S. Kozo, K. Liu, in *Progress in Scale Modeling Vol. II* (Eds.: K. Saito, A. Ito, Y. Nakamura, K. Kuwana), Springer International Publishing, **2015**, pp. 239–248.
[22] K. Marx, O. Bertsch, T. Pröll, H. Hofbauer, *Energy Procedia* **2013**, *37*, 635–644.
[23] F. Gallucci, H. P. Hamers, M. van Zanten, M. van Sint Annaland, *Chem. Eng. J.* **2015**, *274*, 156–168.
[24] K. Mayer, S. Penthor, T. Pröll, H. Hofbauer, *Appl. Energy* **2015**, *157*, 323–329.
[25] J. Ströhle, M. Orth, B. Epple, *Appl. Energy* **2014**, *113*, 1490–1495.
[26] P. Ohlemüller, J.-P. Busch, M. Reitz, J. Ströhle, B. Epple, *J. Energy Resour. Technol.* **2016**, *138*, 042203–042203.
[27] M. L. Szulczewski, C. W. MacMinn, H. J. Herzog, R. Juanes, *Proc. Natl. Acad. Sci. U.S.A.* **2012**, *109*, 5185–5189.
[28] M. C. Payán, B. Verbinnen, B. Galan, A. Coz, C. Vandecasteele, J. R. Viguri, *Environ. Pollut.* **2012**, *162*, 29–39.
[29] E. R. Bobicki, Q. Liu, Z. Xu, H. Zeng, *Prog. Energy Combust. Sci.* **2012**, *38*, 302–320.
[30] S. Bhavsar, M. Najera, G. Veser, *Chem. Eng. Technol.* **2012**, *35*, 1281–1290.
[31] L. F. de Diego, M. Ortiz, J. Adánez, F. García-Labiano, A. Abad, P. Gayán, *Chem. Eng. J.* **2008**, *144*, 289–298.
[32] L. M. Neal, A. Shafiefarhood, F. Li, *ACS Catal.* **2014**, *4*, 3560–3569.
[33] F. He, X. Li, K. Zhao, Z. Huang, G. Wei, H. Li, *Fuel* **2013**, *108*, 465–473.
[34] M. Rydén, A. Lyngfelt, T. Mattisson, *Fuel* **2006**, *85*, 1631–1641.
[35] T. Pröll, J. Bolhàr-Nordenkampf, P. Kolbitsch, H. Hofbauer, *Fuel* **2010**, *89*, 1249–1256.
[36] Q. Zafar, T. Mattisson, B. Gevert, *Ind. Eng. Chem. Res.* **2005**, *44*, 3485–3496.
[37] L. Neal, A. Shafiefarhood, F. Li, *Appl. Energy* **2015**, *157*, 391–398.
[38] A. Shafiefarhood, N. Galinsky, Y. Huang, Y. Chen, F. Li, *ChemCatChem* **2014**, *6*, 790–799.
[39] A. Shafiefarhood, J. C. Hamill, L. M. Neal, F. Li, *Phys. Chem. Chem. Phys.* **2015**, *17*, 31297–31307.

[40] "Rising demand, low-cost feed spur ethylene capacity growth," can be found under http://www.ogj.com/articles/print/volume-112/issue-7/special-report-ethylene-report/rising-demand-low-cost-feed-spur-ethylene-capacity-growth.html, accessed [15 Jan 2016]
[41] C. A. Gärtner, A. C. van Veen, J. A. Lercher, *ChemCatChem* **2013**, *5*, 3196–3217.
[42] M. P. Tao Ren, *Energy* **2006**, *31*, 425–451.
[43] F. Cavani, N. Ballarini, A. Cericola, *Catal. Today* **2007**, *127*, 113–131.
[44] F. Cavani, F. Trifirò, *Catal. Today* **1995**, *24*, 307–313.
[45] M. D. Argyle, K. Chen, A. T. Bell, E. Iglesia, *J. Phys. Chem. B* **2002**, *106*, 5421–5427.
[46] E. M. Thorsteinson, T. P. Wilson, F. G. Young, P. H. Kasai, *J. Catal.* **1978**, *52*, 116–132.
[47] J. A. Sofranko, J. J. Leonard, C. A. Jones, A. M. Gaffney, H. P. Withers, *Catal. Today* **1988**, *3*, 127–135.
[48] C. A. Jones, J. J. Leonard, J. A. Sofranko, *Energy Fuels* **1987**, *1*, 12–16.
[49] J. A. Sofranko, J. J. Leonard, C. A. Jones, *J. Catal.* **1987**, *103*, 302–310.
[50] C. A. Jones, J. J. Leonard, J. A. Sofranko, *J. Catal.* **1987**, *103*, 311–319.
[51] A. M. Gaffney, C. A. Jones, J. J. Leonard, J. A. Sofranko, *J. Catal.* **1988**, *114*, 422–432.
[52] J. A. Sofranko, R. G. Gastinger, C. A. Jones, *Boron-Promoted Reducible Metal Oxides*, **1990**, US4912081 A.
[53] A. Qiao, V. N. Kalevaru, J. Radnik, A. Düvel, P. Heitjans, A. S. H. Kumar, P. S. S. Prasad, N. Lingaiah, A. Martin, *Ind. Eng. Chem. Res.* **2014**, *53*, 18711–18721.
[54] S. A. Al-Ghamdi, M. M. Hossain, H. I. de Lasa, *Ind. Eng. Chem. Res.* **2013**, *52*, 5235–5244.
[55] S. Al-Ghamdi, M. Volpe, M. M. Hossain, H. de Lasa, *Appl. Catal., A* **2013**, *450*, 120–130.
[56] A. H. Elbadawi, M. S. Ba-Shammakh, S. Al-Ghamdi, S. A. Razzak, M. M. Hossain, *Chem. Eng. J.* **2016**, *284*, 448–457.
[57] I. A. Bakare, S. A. Mohamed, S. Al-Ghamdi, S. A. Razzak, M. M. Hossain, H. I. de Lasa, *Chem. Eng. J.* **2015**, *278*, 207–216.
[58] H. Zimmermann, R. Walzl, in *Ullmann Encyclopedia of Industrial Chemistry*, Wiley-VCH Verlag GmbH & Co. KGaA, **2000**.
[59] L. Neal, S. Yusuf, J. Sofranko, F. Li, in *249th National Meeting of the American Chemical Society. ACS*, (Boston, MA) **2015.**
[60] A. Abad, T. Mattisson, A. Lyngfelt, M. Rydén, *Fuel* **2006**, *85*, 1174–1185.
[61] T. W. Elkins, H. E. Hagelin-Weaver, *Appl. Catal., A* **2015**, *497*, 96–106.
[62] A. Malekzadeh, A. K. Dalai, A. Khodadadi, Y. Mortazavi, *Catal. Commun.* **2008**, *9*, 960–965.
[63] Z. C. Jiang, C. J. Yu, X. P. Fang, S. B. Li, H. L. Wang, *J. Phys. Chem.* **1993**, *97*, 12870–12875.
[64] J. S. Ahari, M. T. Sadeghi, S. Zarrinpashne, *J. Nat. Gas Chem.* **2011**, *20*, 204–213.
[65] Y. T. Chua, A. R. Mohamed, S. Bhatia, Appl. Catal., A **2008**, *343*, 142–148.
[66] R. J. Lancee, A. I. Dugulan, P. C. Thüne, H. J. Veringa, J. W. Niemantsverdriet, H. O. A. Fredriksson, *Appl. Catal., B* **2014**, *145*, 216–222.
[67] M. Johansson, T. Mattisson, A. Lyngfelt, *Ind. Eng. Chem. Res.* **2006**, *45*, 5911–5919.

Entry for the Table of Contents (Please choose one layout)

Layout 1:

FULL PAPER

A chemical looping based oxidative dehydrogenation (CL-ODH) process concept is introduced and validated at a lab scale. Under such a cyclic redox scheme, a metal oxide based oxygen carrier is used to selectively combust hydrogen from ethane dehydrogenation, improving equilibrium conversion and supplying heat for the reaction. This scheme can potentially realize high efficiency with low CO_2 and NO_x emissions.

Luke M. Neal, Seif Yusuf[#] , John A. Sofranko, and Fanxing Li, Co-first Author[#], Corresponding Author*,*

Page No. – Page No.

Oxidative Dehydrogenation of Ethane: A Chemical Looping Approach

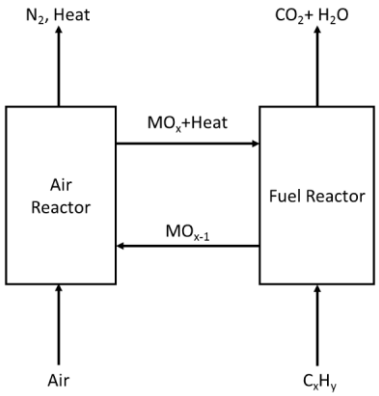

Figure 1

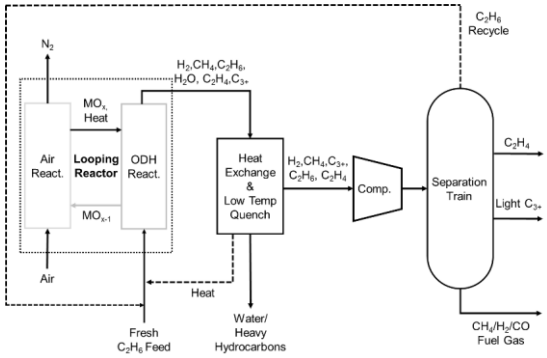

Figure 2

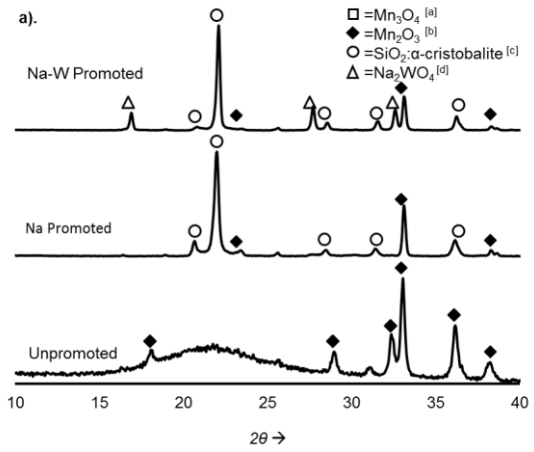

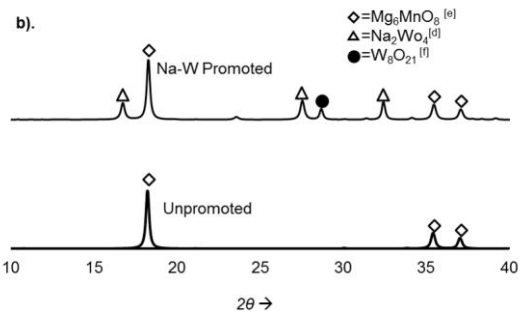

Figure 3

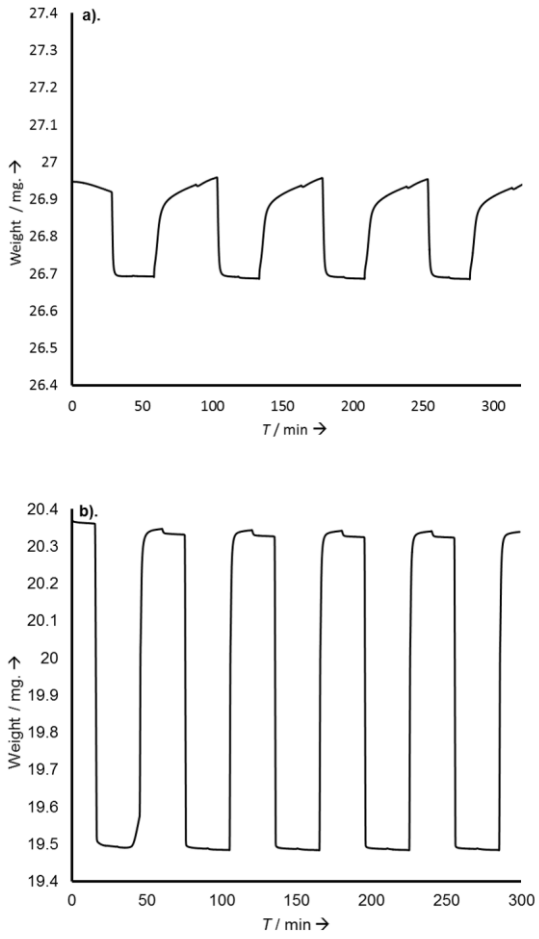

Figure 4

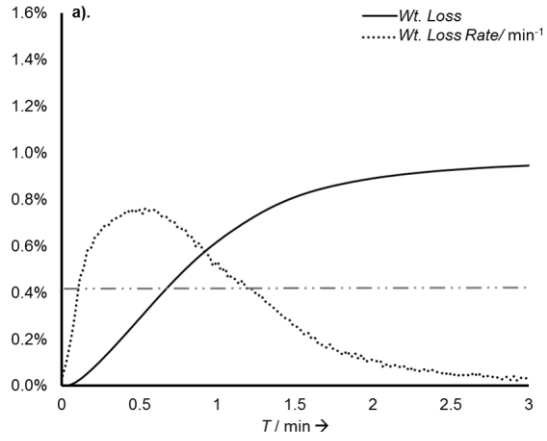

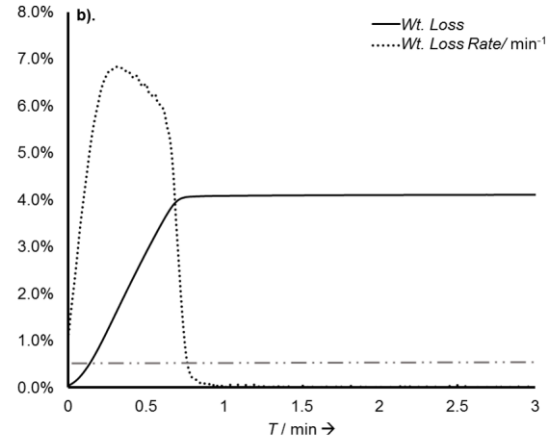

Figure 5

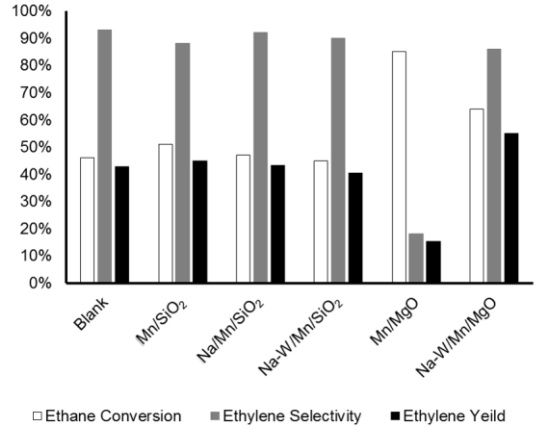

Figure 6

$$\frac{mol\ H_2}{mol\ C_2H_4}\ \frac{r_{O,H_2O}}{r_{O,CO_x}}$$

Table 2 headings

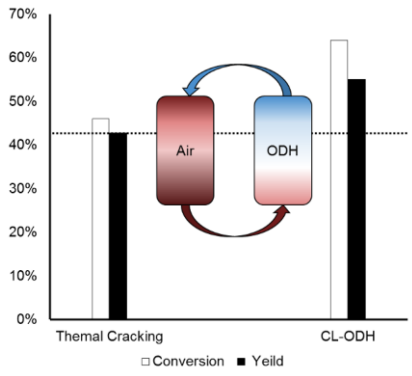

TOC